Maritime Technology and Research

https://so04.tci-thaijo.org/index.php/MTR

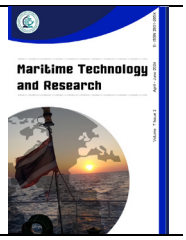

Research Article

Application of CFD to analyze propeller guard kit impact on hydrodynamic performance for long-tail boat propellers in Thailand

Prachakon Kaewkhiaw

Department of Maritime Engineering, Faculty of International Maritime Studies, Kasetsart University, Sriracha Campus, Sri Racha, Chonburi 20230, Thailand

Corresponding author's e-mail address: prachakon.ka@ku.th

Article information

Received: May 9, 2024
Revision: August 14, 2024
Accepted: August 25, 2024

Keywords
Propeller guard kits;
Long-drive shaft;
Inclined shaft propeller;
Long-tail boats;
Unsteady propeller performance;
Cross-flow

Abstract

The propeller guard is a device on the long-drive shaft of long-tail boats which is significant for preventing the propeller from hitting submerged metal or rocks when the boat runs aground in shallow water. There is also a tab device attached to the propeller guard, which alleviates the lifting force in the vertical axial from the propeller force when operating an inclined shaft angle while the boat is at high speed. As a result, the stern of the boat does not raise (reducing the boat's stern trim). Therefore, realistic fluid flow through a long-drive shaft and propeller guard kit is important. This affects the actual performance of the propeller. This research paper proposes the numerical evaluation of propeller performance on a full scale with a long-drive shaft and inclined propeller guard kit using the Reynolds-averaged Navier-Stokes equations (RANS) solver. The SST k-ω turbulence model is adopted to the Reynolds-stress terms in the RANS equations. The computations are performed under oblique flow conditions. The results of propeller performance, pressure distribution, and wake fields around the propeller blades and the propeller guard kit are examined. The results may be used to optimize the shape and characteristics of propeller guard kit for long-tail boats.

1. Introduction

Long-tail boats are native boats in Thailand that have a high speed. The top speed is over 37 knots (68.5 km/h), and the operating speed is approximately 27 knots (50.0 km/h). Therefore, the hull is designed as a planing shape and has a low draft water level. They have been utilized as river passenger vessels. **Figure 1** shows the largest long-tail boat on the Chao Phraya river, the major river in Bangkok, Thailand. This research is focused on medium-sized long-tail boats that are popular in usage, as presented in **Figure 2**. The engine is installed at the boat stern with an inboard, which is connected to a long-drive shaft. The long-drive shaft is covered with a hollow metal rod, which can turn in a semicircle to control the boat's direction without a rudder. The long-drive shaft is connected with an inclination from the horizontal axis. The propeller is set directly on the end of the long-drive shaft. Moreover, most long-tail boats are equipped with an additional propeller guard kit on the long-drive shaft. This is mounted on the long-drive shaft at the propeller front to protect the propeller from hitting submerged metal or rocks when the boat runs aground in shallow water. Additionally, a tab device is attached to the propeller guard to subside the lift force in the vertical axial of the propeller for operating inclined shaft conditions at the boat's high speed. As a result, the stern of the boat does

not raise (reducing trim on the boat stern). The characteristic details of the long-tail boat propeller and the long-drive shaft can be found in the author's previous research (Kaewkhiaw, 2024).

Figure 1 Photograph of long-tail boats on the Chao Phraya river in Bangkok, Thailand.

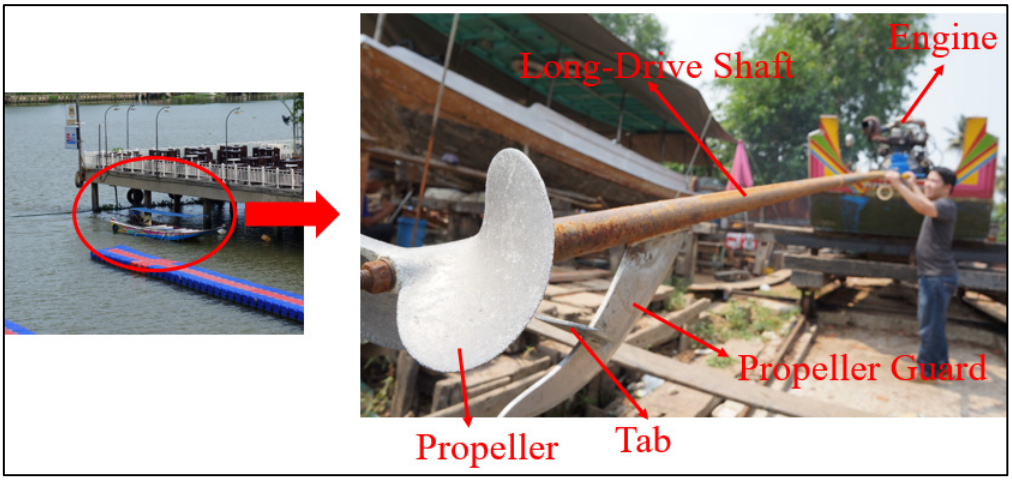

Figure 2 Photograph of long-drive shaft with propeller guard kit.

Many researchers have investigated measurements with inclined shaft conditions. Since these are applied to high-speed ships, research such as in Aktas et al. (2015) has presented the effect of shaft inclination that can induce important unsteady hydrodynamic phenomena, usually associated with small and high-speed craft in cavitation tunnel tests. An experimental study of immersion ratio and shaft inclination angle in the performance of a surface-piercing propeller was conducted by Seyyedi et al. (2019). Ortolani et al. (2019) offered an experimental investigation of single blade loads by captive model tests in pure oblique flow; subsequently, propeller in-plane loads and preliminary comparison of single blade loads during transient phases were described by Ortolani et al. (2021). Next, Efremov (2021) proposed determining the loss of efficiency of twin propeller systems with shaft inclined in circulation maneuvers by appropriate maneuvering experiments with a free-running ship model. Finally, Abbasi et al. (2023) analyzed the flow field around a propeller with an inclined shaft using Laser Doppler Velocimetry (LDV) in the cavitation tunnel.

Concurrently, computational fluid dynamics (CFD) has been widely applied to evaluate the steady and unsteady hydrodynamic performance without/with inclined shaft angles. For example: Seif et al. (2016) performed an unsteady RANS simulation of a surface-piercing propeller in oblique flow. Wang et al. (2017) calculated the unsteady hydrodynamic performance of a DTMB4679 propeller in oblique flow using CFD commercial software code FLUENT. An estimate of the

propeller's performance for a PPTC propeller with an inclined shaft in cavitation conditions, by using a commercial CFD package, was reported by Yilmaz et al. (2017). Gaggero and Villa (2018) presented an analysis of the non-cavitating and cavitating unsteady performances of the Potsdam Propeller Test operating with inclined shaft conditions using the Reynolds-averaged Navier-Stokes equation (RANSE) solver from the open-source OpenFOAM libraries. Kaewkhiaw (2018) investigated propeller performance and wake flow on contra-rotating propellers (CRPs) with steady and unsteady methods in time accuracy based on the Reynolds Averaged Navier-Stokes equations (RANS). A study of the effects of blade pitch ratio on the hydrodynamic performances of a propeller using CFD was conducted by He et al. (2018). Abar and Utama (2019) analyzed the effect of the incline angles for propeller boss cap fins (PBCF) on ship propeller performance with ANSYS CFX code. Boumediene et al. (2019) evaluated the flow around the training ship Seiun-Maru's highly skewed marine propeller (HSP) by assessing blade forces and moments under non-cavitating conditions. The numerical investigation of flow characteristics and hydrodynamic performance of tandem propellers was conducted by Liu and Gong (2020). Paik et al. (2020) examined the changes in the performance of a propeller due to pitch motion using computational fluid dynamics (CFD). Next, the characteristics of propeller cavitation and pressure fluctuation using a numerical simulation of a propeller PC456 in oblique flow based on OpenFOAM software were studied by Zheng et al. (2022). Lastly, Gaggero (2023) investigated the influence of laminar-to-turbulent transition on model scale propeller performance and induced pressure pulses in an unsteady case of oblique flow.

Long-drive shafts are only used on long-tail boats; therefore, literature reviews cannot find anything about long-drive shafts, including propeller guard kits, in previous research by other researchers. However, the authors studied steady and unsteady propeller performance operating at different shaft yaw angle conditions in the first. After that, propeller performance operating at different inclined shaft angle conditions for long-tail boats was investigated by Kaewkhiaw (2020). The aim was to optimize the angles of a long-drive shaft in a boat's operating condition to be the most suitable. In addition, Kaewkhiaw (2021) invented a device to increase the efficiency of the long-tail boat propeller by using boss cap fins (BCF) for application with the propeller using CFD. Recently, drag forces have been created by long-drive shaft characteristics which affect propeller efficiency; this was assessed by Kaewkhiaw (2024).

This has been because most long-tail boats retrofit propeller guard kits on long-drive shafts using their owners' local wisdom, which has not been studied according to theoretical principles. Therefore, this paper aims to examine the effect of fluid flow phenomenon around propeller guard kits before entering the long-tail boat propellers. This will directly influence the propeller efficiency. Computational fluid dynamics (CFD) code Ansys 2024 R1: Ansys Fluent is based on the Reynolds-averaged Navier-Stokes (RANS) equations implemented in this research paper. The calculations were performed with inclined shaft angles and a full-scale propeller size. The results of unsteady performance and propeller efficiency were compared in each case. Pressure distributions on propeller blades and propeller guard kits have been investigated, which confirms their accuracy. In addition, wake fields at the upstream and downstream regions of the long-tail boat propeller were analyzed.

2. Characteristics of the long-drive shaft and the propeller guard kits operating inclined angles

The characteristics of the inflow velocity components, the propeller force generation, the drag force due to the long-drive shaft effect, and the propeller guard kit of a long-tail boat propeller with operating inclined shaft angles are illustrated in **Figure 3**. Inflow velocity, V_{in}, is split into two components in the long-drive shaft plane. The first, $V_{in} \cos\theta$, is in the long-drive shaft axial direction. The second, $V_{in} \sin\theta$, in the vertical direction. θ is the inclined shaft angles from the horizontal axis; meanwhile, the propeller generates the axial thrust, T, in the long-drive shaft plane, which can be divided into two components. First, $T \cos\theta$ is the propeller's thrust force to push the boat hull forward along the horizontal axis. Second, $T \sin\theta$ is the propeller thrust force in the vertical axis, which causes the boat stern to rise. Furthermore, the long-drive shaft and propeller guard kit will create drag

force opposite the propeller's thrust, which increases the boat's resistance at each speed range. Additionally, the tab device on the propeller guard will make a force, $t_{Tab} \sin\theta$ opposite to the propeller thrust, $T \sin\theta$, in the vertical axis. As a result, the net vertical force from the propeller is reduced, especially in high-speed boats. At the same time, the tab device also creates resistance, $t_{Tab} \cos\theta$, in the horizontal axis. Therefore, the total propeller thrust to push the boat hull forward in the horizontal axis is decreased.

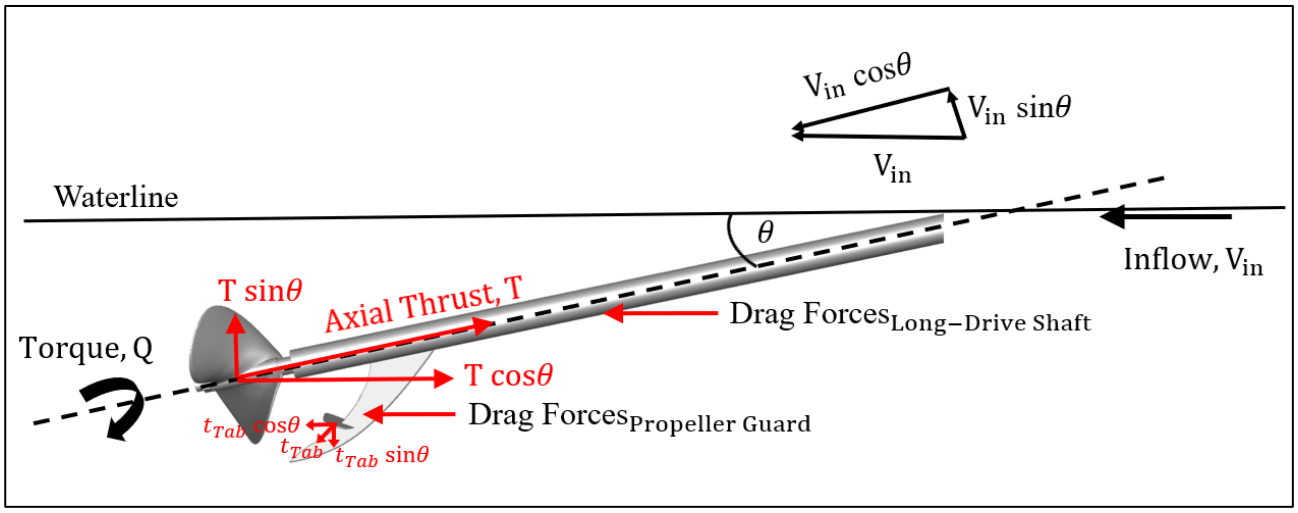

Figure 3 Diagram of inflow velocity components, propeller force generation, drag force from a long-drive shaft, and propeller guard kit of long-tail boat propeller.

3. Numerical formulation

The fluid flow is modeled by enforcing the conservation of mass and momentum equation. The conservation equation is commonly known as the Navier-Stokes equation. It is applied to their incompressible form. Find the Reynolds average; the solution variables in the Navier-Stokes equations of an instantaneous (absolute) solution are decomposed into the mean values (ensemble-averaged or time-averaged) and fluctuating components. For the velocity components:

$$u_i = \bar{u}_i + \acute{u}_i \tag{1}$$

Where $\bar{u}_i$ and $\acute{u}_i$ are the average and fluctuating velocity components ($i = 1, 2, 3$).

Likewise, for pressure and other scalar quantities:

$$\varphi = \bar{\varphi} + \acute{\varphi} \tag{2}$$

Where φ refers to scalars such as pressure, energy, or species concentration.

Substituting an expression of this form for the flow variables in the continuity and momentum equations and using the time averages yields the ensemble-averaged momentum equations. These can be written in Cartesian tensor form as follows (Ansys Fluent Theory Guide, 2024):

$$\frac{\partial \rho}{\partial t} + \frac{\partial (\rho u_i)}{\partial x_i} = 0 \tag{3}$$

$$\frac{\partial (\rho u_i)}{\partial t} + \frac{\partial (\rho u_i u_j)}{\partial x_j} = -\frac{\partial p}{\partial x_i} + \frac{\partial}{\partial x_j}\left[\mu\left(\frac{\partial u_i}{\partial x_j} + \frac{\partial u_j}{\partial x_i} - \frac{2}{3}\delta_{ij}\frac{\partial u_l}{\partial x_l}\right)\right] + \frac{\partial}{\partial x_j}\left(-\rho\overline{u_i' u_j'}\right) \tag{4}$$

Eqs. (3) and (4) are called Reynolds-averaged Navier-Stokes (RANS) equations. They have the same general form as the instantaneous Navier-Stokes equations, where velocities and other solution variables now represent ensemble-averaged or time-averaged values. Further, terms appear that represent the effects of turbulence. These Reynolds stresses, $-\rho\overline{u_i'u_j'}$, must be modeled to close Eq. (4). For flow with variable density, Eqs. (3) and (4) can be interpreted as the Favre-averaged Navier-Stokes equations, where velocity represents the averaged mass. Thus, Eqs. (3) and (4) can be applied to flows with variable density.

The SST *k-ω* model has all the refinements of the baseline (BSL) *k-ω* model, and also takes into account the turbulence shear stress transport in the definition of the turbulent viscosity. It has a well-known high sensitivity to free-stream conditions. The SST *k-ω* model is employed in the present research, which is used to model Reynolds stress in RANS equations. This can be written as follows:

$$\frac{\partial}{\partial t}(\rho k) + \frac{\partial}{\partial x_i}(\rho k u_i) = \frac{\partial}{\partial x_j}\left(\Gamma_k \frac{\partial k}{\partial x_j}\right) + G_k - Y_k + S_k + G_b \tag{5}$$

$$\frac{\partial}{\partial t}(\rho \omega) + \frac{\partial}{\partial x_i}(\rho \omega u_i) = \frac{\partial}{\partial x_j}\left(\Gamma_\omega \frac{\partial \omega}{\partial x_j}\right) + G_\omega - Y_\omega + D_\omega + S_\omega + G_{\omega b} \tag{6}$$

In these equations, the term G_k represents the production of turbulence kinetic energy, and is defined in the same manner as in the standard *k-ω* model. G_ω represents the generation of ω. Γ_k and Γ_ω represent the effective diffusivity of k and ω, respectively. Y_k and Y_ω represent the dissipation of k and ω due to turbulence. D_ω represents the cross-diffusion term. S_k and S_ω are user-defined source terms. G_b and $G_{\omega b}$ account for buoyancy terms, as described in the effects of buoyancy on turbulence in the k-ω models.

The governing equations are solved using the finite volume method with a second-order accuracy discretization technique implemented by Ansys Fluent. The SIMPLE (Semi-Implicit Method for Pressure-Linked Equations) algorithm is selected to solve the pressure-velocity coupling. The gradient of spatial discretization is defined by using the Least Squares Based approach. The pressure-based solver is determined by the second-order scheme. The discretization scheme of momentums is imposed by the Second Order Upwind. Further details are available in the Ansys Fluent Theory Guide (2024).

4. Boundary conditions and numerical grids

Fluid flow entering a long-tail boat propeller operating with inclined shaft angles is unbalanced. This is due to the cross-flow components from the influx of the long-drive shaft and propeller guard kit. Thus, the computational domain in this case cannot be determined in the periodic boundary condition technique for saving calculation time. Therefore, the numerical domain is performed as whole domains with inclined flow conditions. The domains are split into the static fluid domain (stationary) and the dynamic fluid domain (rotation). First, the stationary domain is motionless. Second, the rotation domain is the propeller that rotates with steady states by the moving reference frame (MRF), which is the imagery of fictitious volumetric forces corresponding to inertial forces from the rotational motion.

The computational whole domain in the full-blade of a long-tail boats propellers with a long-drive shaft and propeller guard kit operating with inclined shaft angles is illustrated in **Figure 4**. The inflow velocity, V_{in} is divided into the shaft axial direction, $V_x = V_{in}\cos\theta$, and the shaft vertical direction, which is defined as $V_y = V_{in}\sin\theta$. The inclined angles of the long-drive shaft, θ, are imposed at 12° from the horizontal axis in this case, which is the same as the actual usage of a long-tail boat. The outlet is determined as the pressure outlet on the far field. The turbulence intensity and turbulence viscosity ratio at the inlet condition are set to 1%. The mathematical domain dimensions have been studied in the author's previous research (Kaewkhiaw, 2024). Thereby, the static fluid

domain (stationary), such as diameter (D2) and length (L2), are determined to be equal to 8.8D and 27.1D, respectively. In the dynamic fluid domain (rotation), the diameter (D1) and length (L1) are defined as 1.5D and 1.2D, respectively, where D is the long-tail boat propeller diameter.

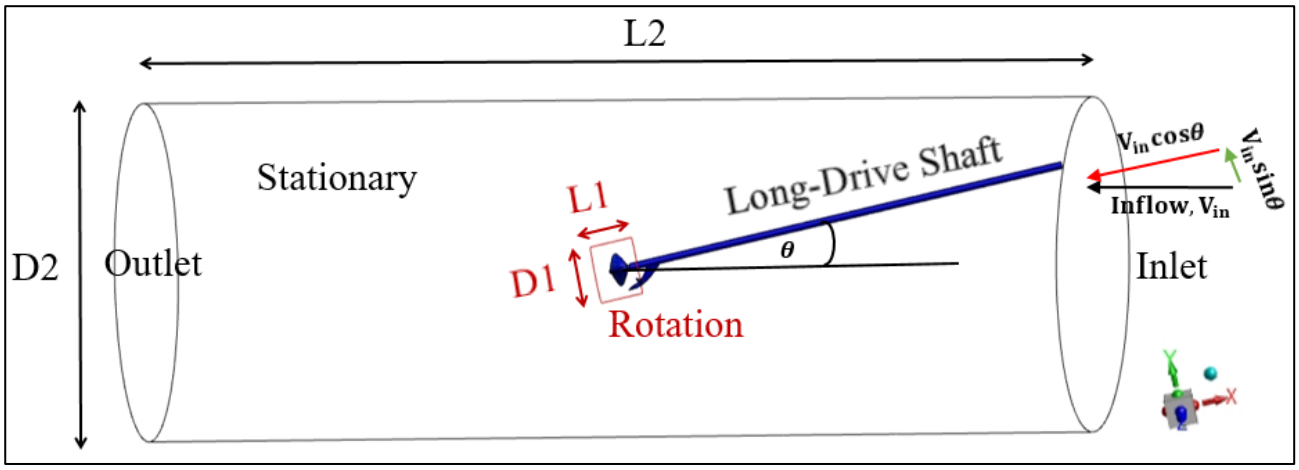

Figure 4 Computational domain of a long-drive shaft and propeller guard kit operating with inclined shaft angles for long-tail boat.

The grid of computational domains (stationary and rotation) is generated by polyhedral cells. The grid quality has been evaluated to guarantee the preciseness of calculation results. They are divided into three conditions. The first is a baseline grid, called Mesh-1. After that, Mesh-1 is improved and called Mesh-2. Finally, Mesh-2 is refined into a finesse grid, called Mesh-3. The total grid, with Mesh-1, Mesh-2, and Mesh-3, is determined to be approximately 2.8M, 5.6M, and 7.5M cells, respectively. The grid independence details under the numerical domain of a long-drive shaft and propeller guard kit operating with inclined shaft angles in full-scale size for a long-tail boat propeller are presented in **Table 1**. The grid refinement of computational domains with the stationary and rotation parts is demonstrated in **Figure 5**. **Figure 6** shows the finesse polyhedral grid for the long-tail boat propeller with long-drive shaft and propeller guard kit for the Mesh-3 condition.

The numerical domains of stationary and rotation parts are separated into discrete control volumes by the polyhedral grids, which are highly flexible and suitable for long-tail boat propellers with long-drive shafts and propeller guard kits. The solid surfaces on the propeller, long-drive shaft, and propeller guard kit are shown by the refinement grids. The boundary prism layers on near solid surfaces, to solve the viscous layer problem, are conducted. A grid on the surrounding area of the solid surfaces defines a larger grid. In addition, the adaptive grid refinement techniques are applied to adjust the grid quality. The first layer thickness of the prism layer by a non-dimensional wall distance on the solid surfaces is prescribed. The other layers are determined to grow the rate of prism layer thickness. The mean values of Y-plus on the location of the first grid point at a distance from the solid surfaces are defined to be nearly 1. The surrounding areas are treated below 30 for the finesse grid, corresponding to the ITTC recommended procedures and guidelines, section 7.5-03-02-03 (2011).

The computational calculations are performed by Ansys 2024 R1: Ansys Fluent, on a personal computer with a 64-bit operating system, x64-based processor, AMD Ryzen 7, PRO 3700, 8-Core Processor@3.6 GHz, and 32 GB of RAM. Computation processing by a parallel processor (16 CPUs) achieves the residual continuity equation convergence requirements of 0.000001.

Table 1 Systematical refinement grids of calculation domain for long-tail boat propellers with long-drive shafts and propeller guard kits operating with inclined shaft angles.

Grid Configuration	Mesh-1 [Baseline grid]	Mesh-2 [Improved grid]	Mesh-3 [Finesse grid]
Grid type	Polyhedral	Polyhedral	Polyhedral
Dynamic fluid domain (rotation)	1.5 M	3.3 M	4.2 M
Static fluid domain (stationary)	1.3 M	2.3 M	3.3 M
Total	2.8 M	5.6 M	7.5 M

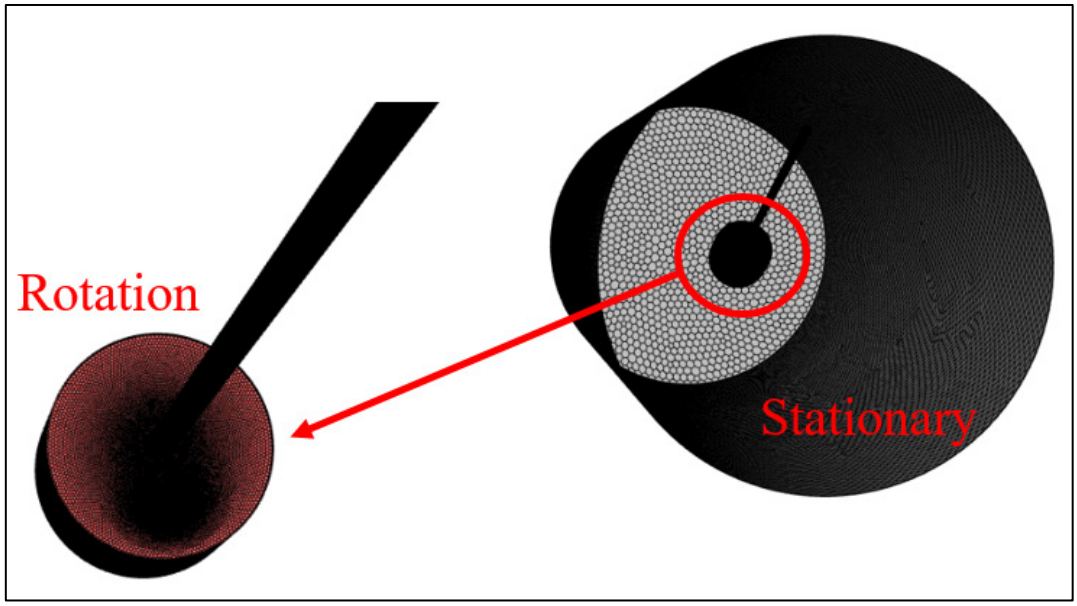

Figure 5 Grid of calculation domains for stationary and rotation parts.

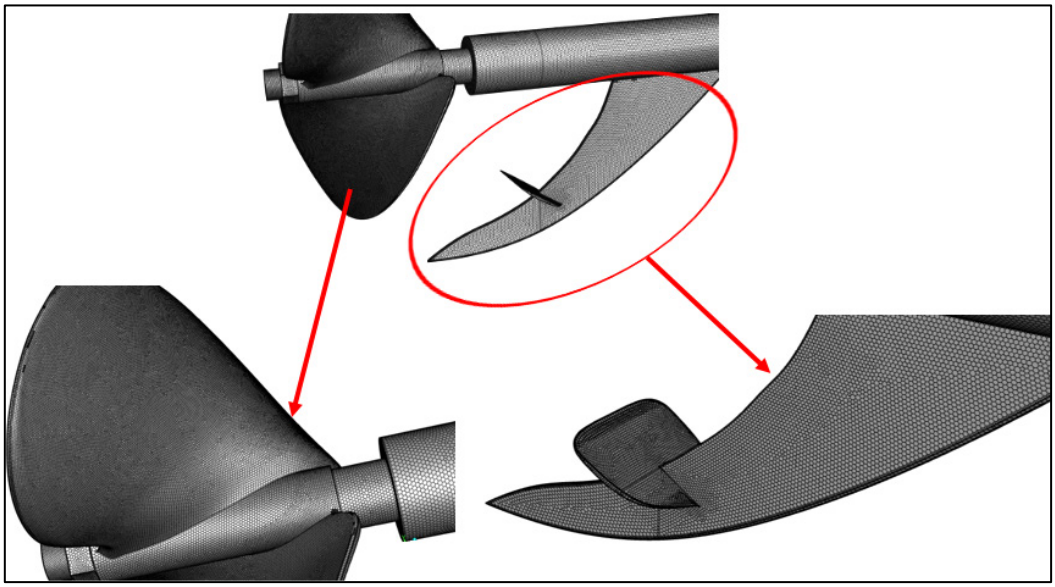

Figure 6 Polyhedral grids on long-tail boat propeller with long-drive shaft and propeller guard kit operating with inclined shaft angles.

5. Description of test problems

Propeller performance is given in the non-dimensional forms of the thrust coefficient [K_T], the torque coefficient [K_Q], and the propeller efficiency, [η_o]. It is defined as follows:

$$K_T = \frac{T}{\rho n^2 D^4} \quad (7)$$

$$K_Q = \frac{Q}{\rho n^2 D^5} \quad (8)$$

$$J = \frac{V_A}{nD} \quad (9)$$

$$\eta_o = \frac{J}{2\pi}\frac{K_T}{K_Q} \quad (10)$$

Where T is the thrust, Q is the torque, n is the propeller rotational speed, J is the advance coefficient, V_A is the inflow velocity, ρ is the water density, η_o is the propeller efficiency, and D is the propeller diameter.

6. Results and discussion

Open water propeller performance of the long-tail boat propeller without a long-drive shaft or propeller guard kit was tested by Kaewkhiaw et al. (2016). First, the numerical results are validated with measurement data, as shown in **Figure 7**. It is found that the tendency of thrust, torque coefficients, and propeller efficiency for computational results using the finesse grid [Mesh-3] condition (black dotted line) are in excellent agreement with the experiment (black circle). Furthermore, the results of propeller performance are very good at the design point (J = 1.1) between the numerical and experimental results. The results of propeller performance with a long-drive shaft operating with inclination (blue dotted line), such as the thrust and torque coefficients, show the calculation values are similar to those measured in open water test conditions at the advance coefficient, $J \leq 0.9$ (low speed). However, the thrust and torque coefficients are increased from the experiment at the advance coefficient, $J \geq 0.9$ (high speed). Especially, the trend of torque coefficient has greatly increased. The torque coefficient deviation range from the experimental data is between 11.71 - 22.83 % at the advance coefficient, J = 1.0 - 1.4. Because of this, propeller efficiency is decreased from the measured data at each range of advance coefficient, [J]. The reason for this result is due to the effect of a long-drive shaft; it obstructs fluid flow entering the propeller, and creates drag forces by itself. This has a significant impact at high speeds.

The comparison of calculation results for long-tail boat propeller performance with a long-drive shaft operating with inclined shaft angles without a guard device case, with a guard device case, and with a guard + tab device case are compared to each other, as shown in **Figure 8**. It is found that the results of propeller performance using finesse grid [Mesh-3] condition in terms of thrust and torque coefficients without guard device case (blue dotted line) shows values higher than those with guard device case (red square dashed line) at each range of advance coefficient, [J]. As a result, propeller efficiency without guard device case is higher than with guard device case. The trend of thrust and torque coefficients with guard + tab device case (green triangle dashed line) is lower than those with guard device case (red square dashed line) including the without guard device case (blue dotted line) at each range of advance coefficient, [J] including at the design point, [J = 1.1]. Therefore, the trend of propeller efficiency with guard + tab device case shows the lowest values compared to each other. This is because the guard device blocks and redirects the direction of the fluid flow that enters the long-tail boat propeller. As a result, the propeller's ability to generate thrust is reduced, which causes the propeller's efficiency to decrease. However, the guard device protects propeller damage from hitting submerged metal or rocks when the boat runs aground in shallow water.

Moreover, a tab device is also installed on the guard device. The tab device will also create the drag force opposite to the propeller thrust in the boat's running direction, corresponding to **Figure 3**. However, the advantage of a tab device is that it generates a force opposite to the propeller thrust in the vertical axis ($T \sin\theta$), which helps to reduce the rise of the boat's stern. The above results show that the guard + tab device has a more negative effect on the propeller efficiency at high speeds than at low speeds. Due to the high speed, the guard + tab device will generate more acting forces than at low speed.

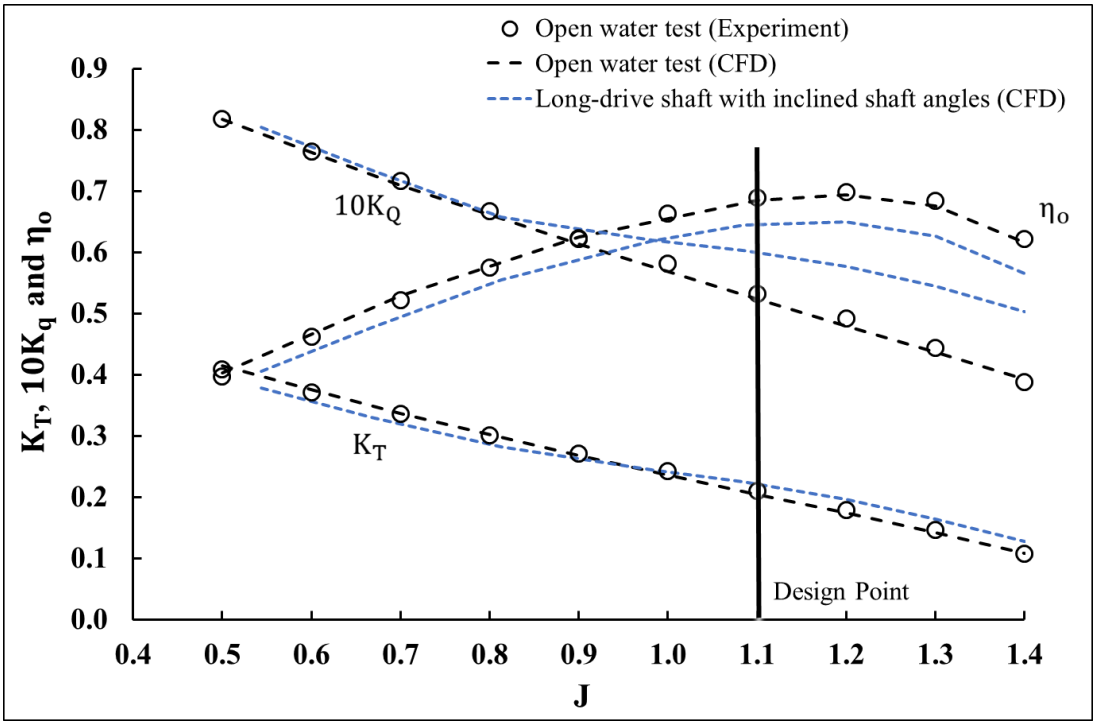

Figure 7 Propeller performances of long-tail boat in open water conditions and long-drive shaft with inclination.

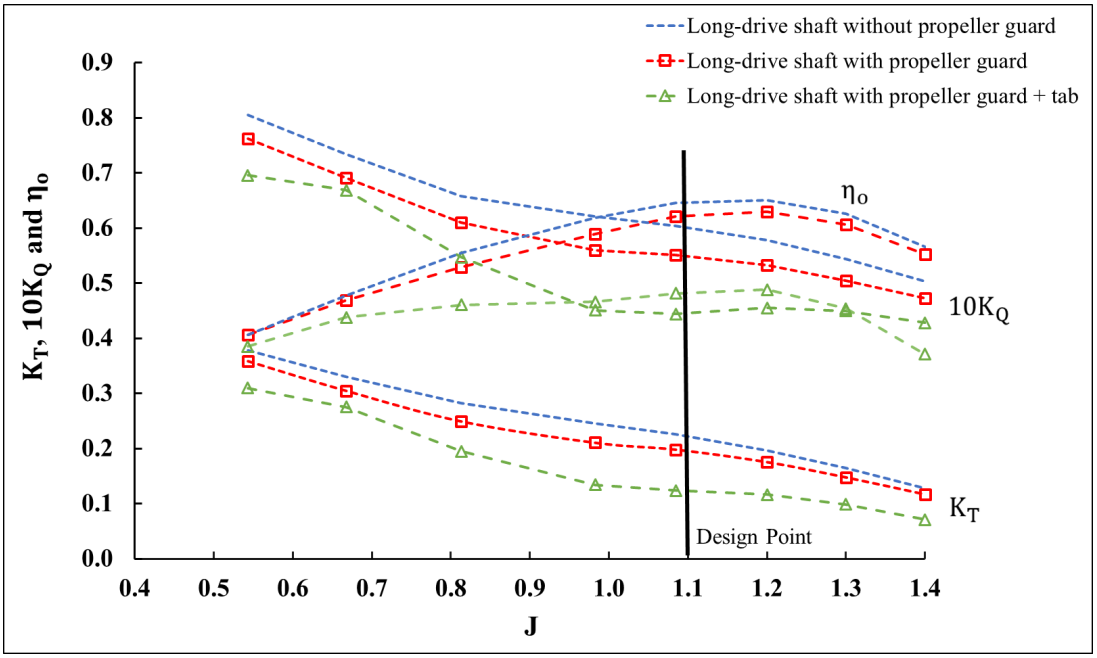

Figure 8 Comparison of long-tail boat propeller performances with long-drive shaft operating with inclination: without and with guard device cases, and with guard + tab device case.

Table 2 presents the actual thrust generation by each device on a long-drive shaft system for a long-tail boat under sea trial tests. It is found that various devices created the drag force opposite to the propeller thrust in the boat's running direction, which affected the increase in the total resistance. It can be seen that the percentage of reduction for total thrust between with versus without (guard + tab) device is increased when the advance coefficient increases (high speed). The range of reduction percentage is equal to 6.33 - 31.7 % which is aggressive. However, the total thrust is reduced by approximately 17.34 % at the design point, [J = 1.1] which is considered severe. This is one of the reasons for its reduced efficiency.

The real torque generated by each device on a long-drive shaft system for the long-tail boat in sea trial tests is illustrated in **Table 3**. The trend of propeller torque seems to have a good relationship with the propeller thrust generation. It is found that the hub and a long-drive shaft generated a small amount of torque. The guard + tab device does not create the torque, because it is motionless. The majority of torque value depends on the propeller, and it is increased when the advance coefficient, [J], is high.

The performance generated by each device on a long-drive shaft system for the long-tail boat in sea trial tests is demonstrated in **Table 4**. The values of the total thrust coefficient, [K_T], with the guard + tab device is lower than those without the guard + tab device at each range of advance coefficients, [J]. As a result, the percentage of total efficiency with the guard + tab device is lower than those without the guard + tab device. In addition, the percentage of total efficiency with the guard + tab device is severely reduced at the high advance coefficient, [J] (high speed). The range of total efficiency reduction between with and without (guard + tab devices) is found to be 6.33 to 31.70 %. However, this dropped by about 17.34 % at the design point, [J = 1.1], which is considered very high.

Table 2 Thrust of each device on long-drive shaft systems in sea trial tests.

	Equipment details					**Total Thrust [T]**		
J	**Propeller (1)**	**Hub (2)**	**Long-drive shaft (3)**	**Guard device (4)**	**Tab device (5)**	**Without (guard + tab) device**	**With (guard + tab) device**	**Reduction**
						(1)+(2)+(3)= (6)	**(1)+(2)+(3)+ (4)+(5) = (7)**	$\left[\frac{(7)-(6)}{(6)}\right] \times 100$
	Thrust (N)	**Thrust (N)**	**Thrust (N)**	**Thrust (N)**	**Thrust (N)**	**Thrust (N)**		**% of reduction**
0.5	2,308.82	-49.59	-17.95	-78.41	-63.53	2,241.28	2,099.34	-6.33
0.7	2,444.13	-45.58	-32.30	-93.15	-74.49	2,366.25	2,198.61	-7.08
0.8	2,063.60	-38.39	-54.97	-105.46	-93.24	1,970.23	1,771.53	-10.09
1.0	2,387.92	-44.14	-123.50	-162.88	-172.24	2,220.28	1,885.15	-15.09
1.1	3,213.46	-54.49	-210.72	-230.76	-280.37	2,948.24	2,437.11	-17.34
1.2	3,843.73	-58.41	-313.55	-285.41	-401.02	3,471.76	2,785.32	-19.77
1.3	4,152.19	-62.42	-433.68	-344.79	-528.31	3,656.09	2,783.00	-23.88
1.4	4,153.31	-65.55	-596.23	-420.97	-685.68	3,491.53	2,384.89	-31.70

Table 3 Torque of each device on long-drive shaft systems in sea trial tests.

J	Equipment details			Total Torque [Q]
	Propeller (1)	Hub (2)	Long-drive shaft (3)	With/Without (guard + tab) device
				(1)+(2)+(3)
	Torque (N·m)	Torque (N·m)	Torque (N·m)	Torque (N·m)
0.5	160.31	-0.02	0.00	160.29
0.7	181.40	-0.02	0.00	181.38
0.8	169.13	-0.01	0.00	169.12
1.0	214.91	-0.01	0.00	214.90
1.1	297.18	-0.01	0.00	297.17
1.2	370.35	-0.01	0.00	370.34
1.3	431.22	0.00	0.01	431.22
1.4	486.97	0.01	0.01	486.98

Table 4 Performance of each device on long-drive shaft systems in sea trial tests.

The sea trial conditions				Total thrust coefficient [K_T]		Total torque coefficient [$10K_Q$]	% of total efficiency [η_o]		
J	N (rpm)	D (m)	Vin (m/s)	Without (guard + tab) device	With (guard + tab) device	With/Without (guard + tab) device	Without (guard + tab) device	With (guard + tab) device	% of reduction
				(1)+(2)+(3)	(1)+(2)+(3) +(4)+(5)	(1)+(2)+(3)	(1)+(2)+(3) = (6)	(1)+(2)+(3) +(4)+(5) = (7)	$\left[\frac{(7)-(6)}{(6)}\right] \times 100$
0.5	1,353.30	0.34	4.17	0.33	0.31	0.70	0.41	0.39	-6.33
0.7	1,468.40	0.34	5.56	0.30	0.28	0.67	0.47	0.44	-7.08
0.8	1,567.20	0.34	7.22	0.22	0.19	0.55	0.51	0.46	-10.09
1.0	1,945.90	0.34	10.83	0.16	0.13	0.45	0.55	0.47	-15.09
1.1	2,305.30	0.34	14.17	0.15	0.12	0.44	0.58	0.48	-17.34
1.2	2,543.10	0.34	17.29	0.15	0.12	0.45	0.61	0.49	-19.77
1.3	2,761.00	0.34	20.34	0.13	0.10	0.45	0.60	0.45	-23.88
1.4	3,005.40	0.34	23.84	0.10	0.07	0.43	0.54	0.37	-31.70

Where: Propeller = (1), Hub = (2), Long-drive shaft = (3), Guard device = (4), Tab device = (5).

Figure 9 shows the pressure coefficient distributions on propeller blades at suction and pressure sides operating with inclined shaft angles at the design point, [J = 1.1], for without and with (guard + tab device). The pressure distribution shapes on each propeller blade at the suction and pressure sides differ because each blade generates an unstable force due to the cross-flow with the inclined shaft angles. For both cases (without and with guard + tab device), the shape of pressure distribution indicates that the pressure value at the blade's downward position is higher than the blade's upward position at the suction side. On the contrary, the shape of pressure distribution at the blade's downward position is lower than the blade's upward position at the pressure side. As a result, vibration and cavitation may occur. This causes damage to the long-tail boat propeller. In addition, the guard + tab device also showed a higher average pressure distribution on each propeller blade than without the guard + tab device on the suction and pressure sides. This is because the guard + tap device hinders the fluid flow before entering the propeller.

The pressure coefficient distribution for a long-drive shaft operating with inclined angles at the design point, [J = 1.1], for without and with (guard + tab device) is shown in **Figure 10**. It can be seen that the high pressure is generated at the rear of the guard device because of its proximity to the rotating propellers. Therefore, its pressure fluctuates in these areas.

The pressure coefficient distribution on the guard device at the high-pressure and low-pressure regions for a long drive shaft operating with inclination at the design point, [J = 1.1], is demonstrated in **Figure 11**. It appears that the rear of the guard device on the right-hand side, when looking at the boat forward, has a higher pressure than on the left-hand side of it. This may be influenced by the fluid flow in the direction of propeller rotation. **Figure 12** presents the pressure coefficient distribution of the tab device which is mounted on the guard device operating with inclined angles at the design point, [J = 1.1]. It is found that the upper surface of the tab device creates a high pressure, and the lower surface generates a low pressure. Therefore, the tab device creates a lifting force in the direction of gravity, which helps to reduce the propeller raise force, $(T \sin \theta)$, corresponding to **Figure 3**. Furthermore, it also creates drag forces in the opposite direction to the propeller thrust. Hence, the guard + tab device may adversely affect the term of propeller performance.

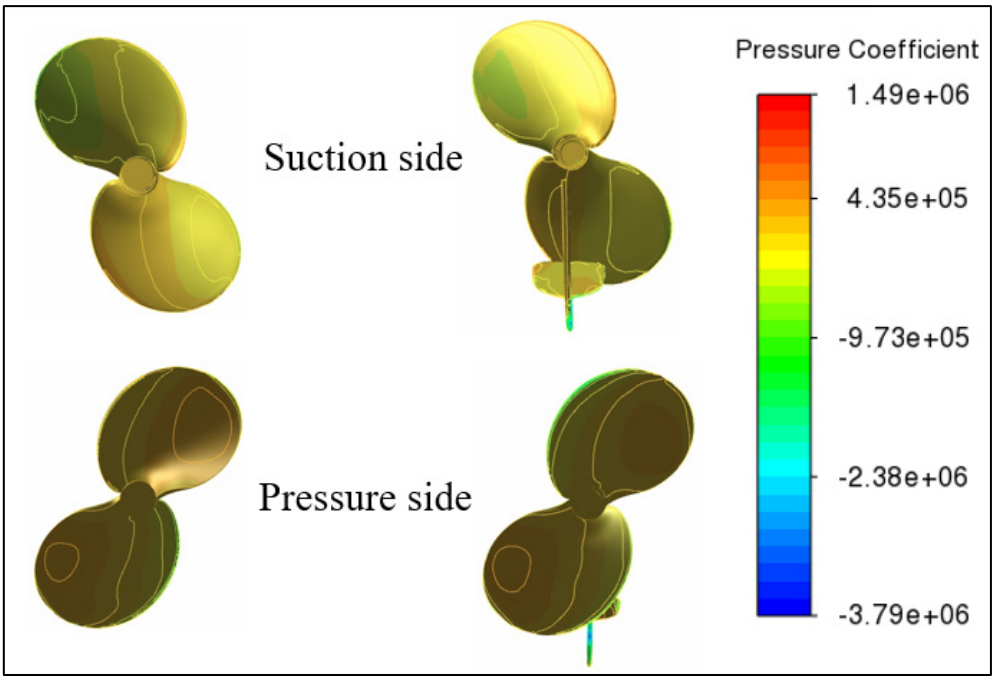

Figure 9 Comparison of pressure coefficient contour lines on propeller blades at suction and pressure sides operating with inclination at the design point, [J = 1.1] between without (left) and with (right) guard + tab devices.

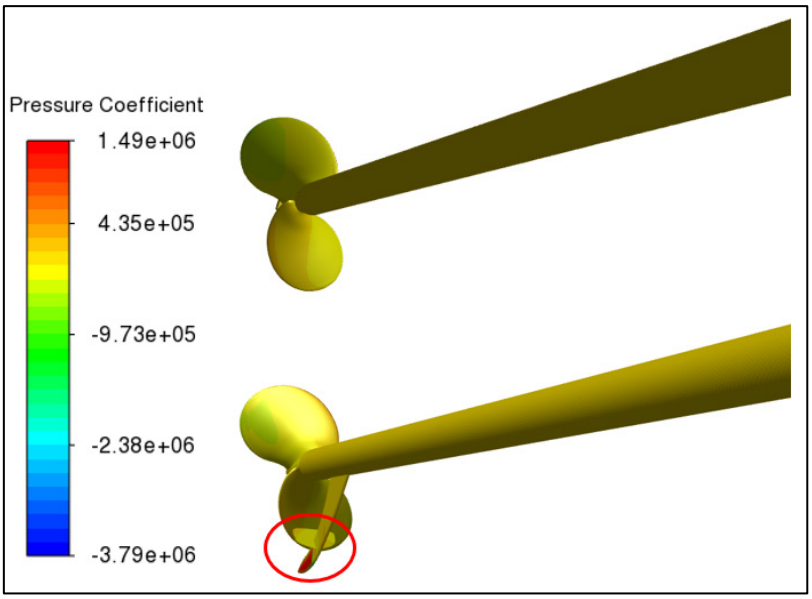

Figure 10 Comparison of pressure coefficient for long-drive shaft operating with inclined shaft conditions at design point, [J = 1.1], between without (upper) and with (lower) guard + tab device.

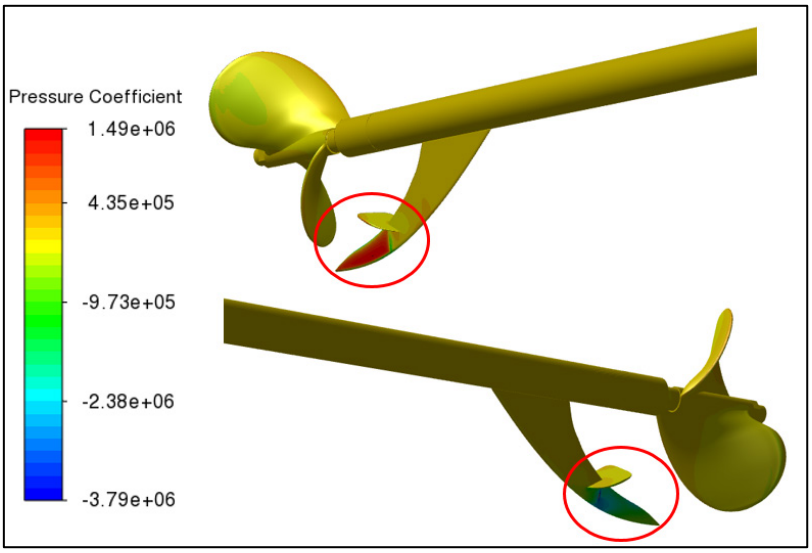

Figure 11 Pressure coefficient for long-drive shaft operating with inclined shaft conditions at design point, [J = 1.1], with guard + tab device: high-pressure area (upper) and low-pressure area (lower).

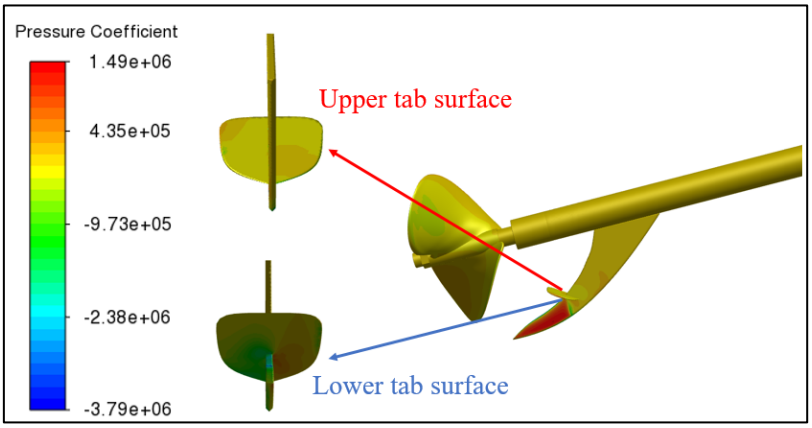

Figure 12 Pressure coefficient on upper and lower of tab surfaces for long-drive shaft operating with inclined shaft angles at design point, [J = 1.1].

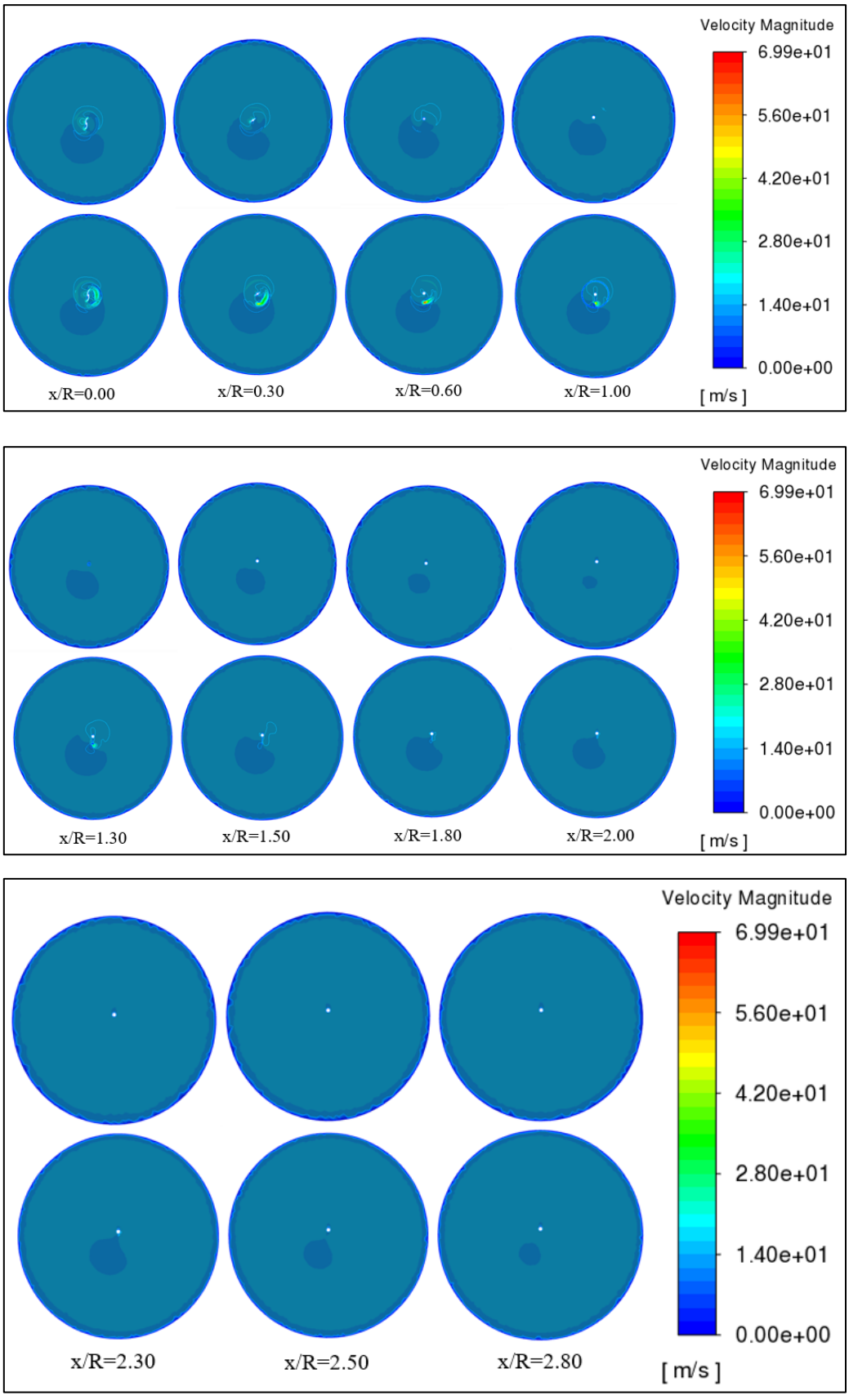

Figure 13 Comparison of velocity magnitude at upstream regions for a long-drive shaft operating with inclination at design point, [J = 1.1], in position, x/R = 0.00 - 2.80, between without (upper) and with (lower) guard + tab devices.

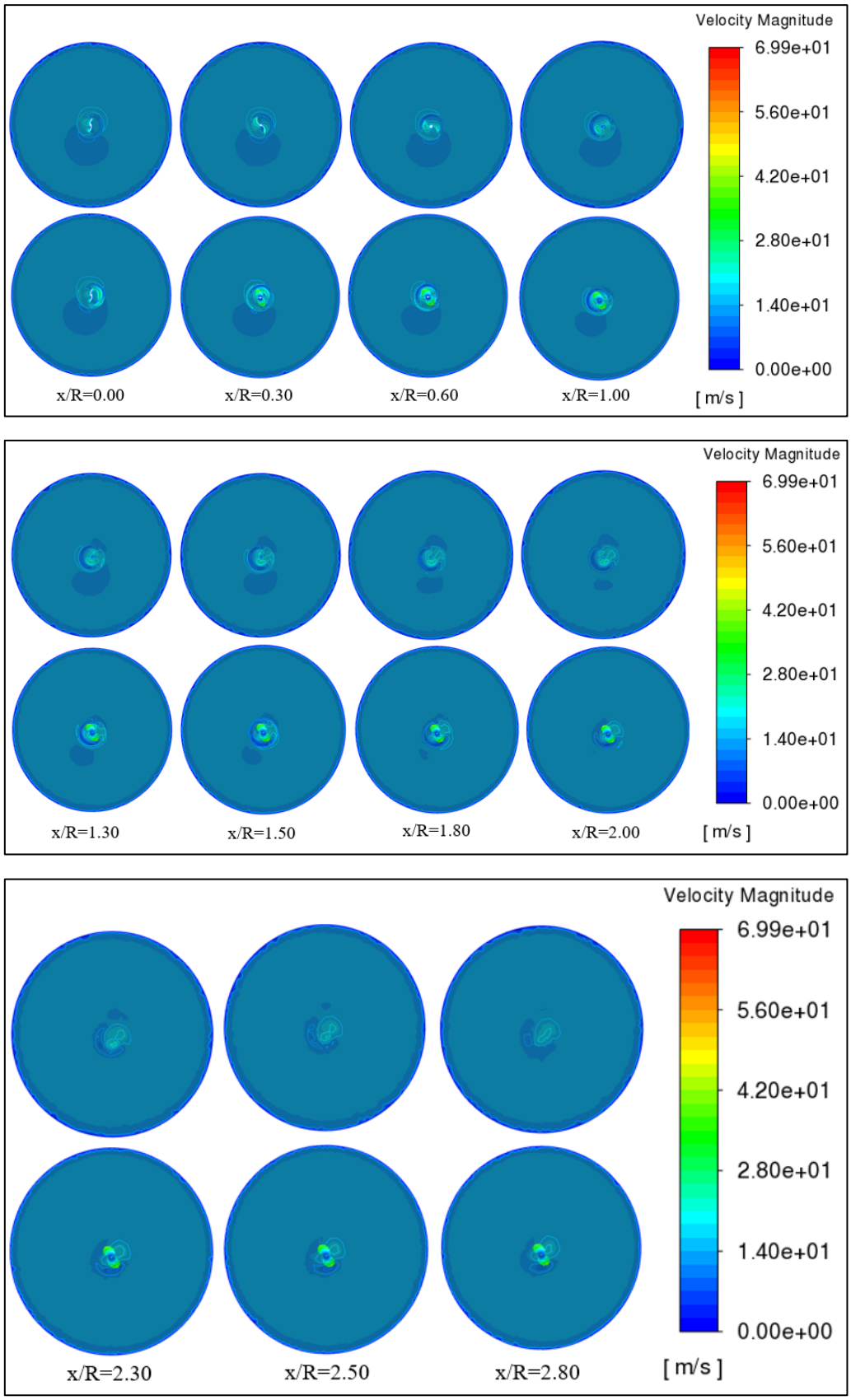

Figure 14 Comparison of velocity magnitude at downstream regions for long-drive shaft operating with inclination at design point, [J = 1.1], in position, x/R = 0.00 - 2.80, between without (upper) and with (lower) guard + tab devices.

The wake fields of a long-drive shaft operating with inclined angles at the design point, [J = 1.1], are analyzed through the velocity magnitude contour lines. The axial velocity field at upstream regions of the long-tail boat propeller in the cutting plane crossing the propeller center at x/R = 0.00 to 2.80 for without and with the guard + tab devices are displayed in **Figure 13**. It seems that the average velocity contours for operating with the guard + tab device at the center of the propeller plane, (x/R = 0.00), and adjacent to the propeller center, (x/R > 0.00), planes showed more than operating without the guard + tab device. Because the guard + tab device disturbs the flow field before entering the propeller, this causes the flow to become more turbulent, resulting in a high velocity. This is the reason why the propeller efficiency is reduced when working with the guard + tab device.

The axial velocity fields at downstream regions of the long-tail boat propeller in the cutting plane crossing the propeller center at x/R = 0.00 to 2.80 for without and with the guard + tab devices are shown in **Figure 14**. The average velocity shape for operating with the guard + tab device in each position appears to be greater than those for operating without the guard + tab device.

7. Conclusions

The computational results of propeller performance for a long-tail boat in open water conditions are compared with experimental data. It is found that the calculation results are highly accurate at each range of advance coefficients, [J], as well as at the design point, [J = 1.1]. The propeller efficiency of a long-drive shaft operating with inclined shaft angles is lower than that for operating without inclined shaft angles at each range of advance coefficients, [J]. This is because a long-drive shaft obstructs the fluid flow entering the propeller and creates drag forces on its own. Therefore, there is a significant impact when the boat is at high speed.

The comparison of propeller performance of a long-drive shaft operating with inclined shaft angle conditions is as follows: without the guard device, with the guard device, and with the guard + tab device. The results in terms of thrust, torque coefficients, and propeller efficiency for those without the guard device are higher than those with the guard device at each range of inflow speed. Moreover, the values of propeller performance for those with the guard + tab device are lowest when compared to those with the guard device and those without the guard device at each range of advance coefficients, [J]. The range of total efficiency reduction between operating with the guard + tab device and operating without the guard + tab device is found to be 6.33 - 31.7 %, which is highly influential to total efficiency. However, it is decreased by approximately 17.34 % at the design point, [J = 1.1], which is the operating speed of the Thai long-tail boat. It is highly negative to the propulsion system. This is because the guard device blocks and redirects the direction of the fluid flow into the long-tail boat propeller. As a result, the propeller's ability to generate thrust is reduced, which causes the propeller's efficiency to decrease. In addition, the tab device is also mounted on the guard device. It also creates a drag force opposite to the propeller's thrust in the boat's running direction. However, the advantage of a tab device is that it generates a force opposite to the propeller thrust in the vertical axis, which helps to reduce the rise of the boat's stern. As a result, it has been shown that the guard + tab device harms the propeller efficiency at high speeds more than at low speeds. The average pressure coefficient on each propeller blade for those with the guard + tab device is mostly more extreme than those without the guard + tab device. Additionally, the mean velocity magnitudes at upstream and downstream regions confirm that the guard + tab device has obstructed and changed the flow field route into the propeller, influencing propeller efficiency.

The results of this study show that the guard + tab device on a long-drive shaft can prevent propeller damage when the boat runs aground in shallow water. However, this negatively affects propeller efficiency, which causes more fuel consumption in Thai long-tail boats. It should be appropriately considered from the beginning for designing the shapes and characteristics in working conditions, because they will directly affect propeller efficiency. Therefore, CFD is a useful tool that gives an understanding of the fluid flow behavior in this case. This contributes to optimizing the shape of the guard + tab device.

References

Abar, I. A. C., & Utama, I. K. A. P. (2019). Effect of the incline angle of propeller boss cap fins (PBCF) on ship propeller performance. *International Journal of Technology, 10*(5), 1056-1064. https://dx.doi.org/10.14716/ijtech.v10i5.2256

Abbasi, A. A., Franzosi, G., Canepa, E., Gaggero, S., Villa, D., Viviani, M., & Tani, G. (2023). Experimental analysis of the flow field around a propeller with inclined shaft. *Ocean Engineering, 285*, 115-237. https://doi.org/10.1016/j.oceaneng.2023.115237

Aktas, B., Atlar, M., Turkmen, S., Korkut, E., & Fitzsimmons, P. (2015). Systematic cavitation tunnel tests of a Propeller in uniform and inclined flow conditions as part of a round robin test campaign. *Ocean Engineering, 120*, 136-151. http://dx.doi.org/10.1016/j.oceaneng.2015.12.015

Alimirzazadeh, S., Roshan, S. Z., & Seif, M. S. (2016). Unsteady RANS simulation of a surface piercing propeller in oblique flow. *Applied Ocean Research, 56*, 79-91. https://doi.org/10.1016/j.apor.2016.01.003

Ansys Fluent Theory Guide. (2024). *Ansys fluent theory guide*. ANSYS.

Boumediene, K., Belhenniche, S. E., Imine, O., & Bouzit, M. (2019). Computational hydrodynamic analysis of a highly skewed marine propeller. *Journal of Naval Architecture and Marine Engineering, 16*(1), 21-32. http://dx.doi.org/10.3329/jname.v16i1.38757

Efremov, D. (2021). Determining the loss of efficiency of twin propeller systems in circulation maneuvers. *Maritime Technology and Research, 3*(2), 89-101. https://doi.org/10.33175/mtr.2021.244703

Gaggero, S. (2023). Influence of laminar-to-turbulent transition on the model scale propeller performance and induced pressure pulses in an unsteady case of oblique flow. *Journal of Marine Science and Application, 22*, 199-218. https://doi.org/10.1007/s11804-023-00334-w

Gaggero, S., & Villa, D. (2018). Cavitating propeller performance in inclined shaft conditions with OpenFOAM: PPTC 2015 test case. *Journal of Marine Science and Application, 17*, 1-20. https://doi.org/10.1007/s11804-018-0008-6

Kaewkhiaw, P., Yoshitake, A., Kanemaru, T., & Ando, J. (2016). *Evaluation of Thai long-tail boat propeller performance and its improvement*. In Proceedings of the 12th International Conference on Hydrodynamics, Netherland.

Kaewkhiaw, P. (2018). CFD investigation on steady and unsteady performances of contra-rotating propellers. *Journal of Naval Architecture and Marine Engineering, 15*(2), 91-105. https://doi.org/10.3329/jname.v15i2.36225

Kaewkhiaw, P. (2020). CFD analysis of unsteady propeller performance operating at different inclined shaft angles for LONG-TAIL boats in Thailand. *Journal of Naval Architecture and Marine Engineering, 17*(2), 115-127. http://dx.doi.org/10.3329/jname.v17i2.42622

Kaewkhiaw, P. (2021). Numerical study of propeller boss cap fins on propeller performance for Thai Long-Tail Boat. *Ocean Systems Engineering, 11*(4), 373-392. https://doi.org/10.12989/ose.2021.11.4.373

Kaewkhiaw, P. (2024). Effects of a long-drive shaft on flow field around the high-speed boat propeller in Thailand using CFD. *Maritime Technology and Research, 6*(3), 269212. https://doi.org/10.33175/mtr.2024.269212

Liu, Y., & Gong, Q. (2020). Numerical investigation on the flow characteristics and hydrodynamic performance of tandem propeller. *Applied Ocean Research, 101*, 102292. https://doi.org/10.1016/j.apor.2020.102292

Cong, N. C., Loi, L. N., & He, N. V. (2018). A study on effects of blade pitch on the hydrodynamic performances of a propeller by using CFD. *Journal of Shipping and Ocean Engineering, 8*, 36-42. https://doi 10.17265/2159-5879/2018.01.005

Ortolani, F., Viviani, M., Tani, G., & Dubbioso, G. (2019). Experimental investigation of single blade loads by captive model tests in pure oblique flow. *Ocean Engineering, 196*, 106789. https://doi.org/10.1016/j.oceaneng.2019.106789

Ortolani, F., Tani, G., Viviani, M., & Dubbioso, G. (2021). Experimental investigation of single blade loads by captive model tests in pure oblique flow. Part II: Propeller in-plane loads and preliminary comparison of single blade loads during transient phases. *Ocean Engineering, 234*, 109149. https://doi.org/10.1016/j.oceaneng.2021.109149

Paik, K. J., Jang, Y. H., Eom, M. J., Kim, S. H., & Song, G. (2020). A numerical study on the open water performance of a propeller with sinusoidal pitch motion. *Brodogradnja/Shipbuilding*, *71*(1), 71-83. http://dx.doi.org/10.21278/brod71105

Practical Guidelines for Ship CFD Applications. (2011). *Practical guidelines for ship CFD applications*. ITTC Recommended Procedures and Guidelines.

Seyyedi, S. M., Shafaghat, R., & Siavoshian, M. (2019). Experimental study of immersion ratio and shaft inclination angle in the performance of a surface-piercing propeller. *Mechanical Sciences, 10*, 153-167. https://doi.org/10.5194/ms-10-153-2019

Wang, C., Sun, S., Sun., S & Li, L. (2017). Numerical analysis of propeller exciting force in oblique flow. *J Mar Sci Technol*. https://doi10.1007/s00773-017-0431-4

Yilmaz, N., Khorasanchi, M & Atlar, M. (2017). An Investigation into Computational Modelling of Cavitation in a Propeller's Slipstream. *Fifth International Symposium on Marine Propulsion, Espoo, Finland.*

Zheng, C., Hong, F., Zhang, Z & Liu, D. (2022). The Numerical Investigation of Propeller Cavitation Benchmark Tests in Oblique Flow. *Seventh International Symposium on Marine Propulsors, Wuxi, China.*